Journal of Power Sources 219 (2012) 172–179

Contents lists available at SciVerse ScienceDirect

Journal of Power Sources

journal homepage: www.elsevier.com/locate/jpowsour

Computer simulations of topological connectivity of the triple phase boundaries in solid oxide fuel cell composite cathodes

S. Zhang*, A.M. Gokhale

School of Materials Science and Engineering, Georgia Institute of Technology, Atlanta, GA-30332-0245, USA

HIGHLIGHTS

- ► 3D microstructure simulations were generated for composite electrodes.
- ► Particles of different sizes and morphologies were used in simulations.
- ► Process parameters were studied for effects on triple phase boundary connectivity

ARTICLE INFO

Article history:
Received 16 May 2012
Accepted 16 July 2012
Available online 22 July 2012

Keywords:
Triple-phase boundary
Simulation
Solid oxide fuel cell
Microstructure

ABSTRACT

Density of electrochemically active triple phase boundary sites is one of the most important factors that affect the performance of composite cathodes in solid oxide fuel cells. Only the topologically connected triple phase boundaries can become electrochemically active. Therefore, microstructure-based geometric modeling of topologically connected triple phase boundaries is of interest. In this contribution, three-dimensional microstructure simulations are utilized to predict the topological connectivity of the triple phase boundaries in a composite SOFC cathode as a function of the volume fractions of the constituents, particle size, shape, and the thickness of the cathode. The simulations show that the volume fractions of the constituent phases and electrode thickness are the most important factors that affect the topological connectivity. The simulations also reveal the geometric conditions under which most of the triple phase boundaries are topologically connected, so that for such SOFC cathode microstructures, the existing models for total *geometric* triple phase boundary length density can be also used to approximate the length density of the *topologically connected* triple phase boundaries.

1. Introduction

Solid oxide fuel cell (SOFC) is an attractive energy conversion device featuring high energy conversion efficiency [1,2]. An important technological challenge for SOFCs is to lower the operating temperature of the cell (<600 °C), which can increase the long-term stability and decrease the operating cost. In SOFC where yittria-stablized zirconia (YSZ) is used as electrolyte and strontium-doped lanthanum manganite (LSM) is used as cathode, the performance of SOFC is limited by the amount of reaction sites. The oxygen ion conductivity of LSM is limited at low operation temperatures; YSZ is an electron insulator. Therefore, the oxygen reduction reaction, which involves transfer of oxygen gas, electrons and oxygen ions, primarily occurs at one-dimensional lineal junctions common to the LSM, YSZ and gaseous oxidant called triple phase boundaries (TPB) [3,4].

The low temperature catalytic activity (and hence the performance) of the SOFC cathodes can be improved by increasing the length of TPB sites. In the SOFCs having single constituent cathode, it is difficult to increase the length of TPB as they exist only at the planar junction between electrolyte and cathode. However, TPB length can be significantly increased via the use of porous meso-scale [5] or nano-scale [6] composite cathodes containing three phases, namely, electrode (e.g., LSM), electrolyte (e.g., YSZ), and porosity [7–10]. Likewise, the electrochemical activity of SOFC anodes can also be improved by using porous composites containing electronic conductor (e.g., nicole), electrolyte (e.g., YSZ), and porosity.

Numerous theoretical models have been proposed to predict the total geometric TPB length per unit volume of the composite electrode, L_{TPB} [11–14], as a function of the parameters such as constituent volume fractions, and particle size. The most widely used model was developed by Sunde [11]:

* Corresponding author. School of Materials Science and Engineering, Georgia Institute of Technology, 771 Ferst Dr. NW, Rm 288, Atlanta, GA-30332-0245, USA. Tel.: +1 303 596 1817; fax: +1 303 273 3016.
E-mail addresses: szhang@gatech.edu, shenjia.zhang@gmail.com (S. Zhang).

0378-7753/$ – see front matter © 2012 Elsevier B.V. All rights reserved.
http://dx.doi.org/10.1016/j.jpowsour.2012.07.049

$$L_{TPB} = l_{TPB} n Z_{edel} P_c(Z_{eded}) P_c(Z_{elel}) \quad (1)$$

where l_{TPB} is the circumference of the intersect formed by the impingement of the electrode and electrolyte particle; n is the number of electrode particles per unit volume; Z_{edel} is the number of electrolyte particles impinged with one electrode particle; $P_c(Z_{eded})$ and $P_c(Z_{elel})$ are the probabilities of an electrolyte and electrode particle connected to its corresponding conductive network, respectively. Sunde's model has been modified into different forms in other studies [13,14] but the basic assumptions remain: a constant circumference between electrode and electrolyte through-out the composite electrode, percolating porosity and spherical electrolyte and electrode particles of constant radii. Eq. (1) calculates the length of topologically connected[1] TPB per unit volume of a composite electrode. The probability that a site of TPB is topologically connected is given by $P_c(Z_{eded})P_c(Z_{elel})$, where $P_c(Z_{eded})$ and $P_c(Z_{elel})$ are percolating probabilities derived according to percolation theory. Correct calculation of percolating probability requires the average coordinate number of the particle mixture. Sunde [11] assumes the average coordinate number is 6; however, such assumption might be inaccurate in a particle mixture where the radii of particle differ substantial.

Computer simulations have been used to generate more realistic composite electrode microstructures. In simulations of composite electrodes, particles of electrolyte and electrode particles are placed randomly in a spatial lattice [11,15–17] or are close-packed [13,18–20]. In computer simulations, length of TPB is measured either by tracking each individual TPB site or by digital image analysis. The topological connectivity of TPB is determined by examine the topological connectivity of the electrolyte and electrode particles; the connectivity of pores can also be determined by detecting the presence of a connected path of pore pixels.

Computer simulations are not yet free from simplistic geometric assumptions. For example, it is usually assumed that all component particles are spheres, although their shapes are allowed to alter slight to simulate sintering [13,17,19]. It has been shown that flake-like LSM particles can be synthesized [21]. Particle morphologies may affect both total length and connectivity of TPB.

A novel analytical model for the length of TPB in composite electrodes has been developed to capture the effect of particle morphology, size distribution as well as composition and porosity [22]. The total length of TPB is given by

$$L_{TPB} = \frac{\pi}{4} F_1(\alpha) F_2(\theta_P) F_3\left(K\right) F_4(CV, \gamma) \frac{1}{\langle D_Y \rangle \langle D_L \rangle} \quad (2)$$

where $F_1(\alpha)$ captures the effect of composition, or volume fraction ratio (α) between electrolyte and electrode particles; $F_2(\theta_P)$ captures the effect of porosity (θ_P); $F_3(K)$ captures the effect of particle morphology designated by K; F_4(CV,γ) captures the effect of variance (CV) and skewness (γ) in particle size distribution; $\langle D_Y \rangle$ and $\langle D_L \rangle$ are the diameters of electrode and electrolyte particles, respectively. More notably, all functions in Eq. (2) are explicit expressions of the microstructure attributes. The details of the analytical model are given in another contribution [22].

The analytical model (Eq. (2)) calculates the total length of TPB and does not distinguish between isolated and connected TPB. While Eq. (2) is convenient for optimization of the total length of TPB, it is important to determine the connectivity of TPB in analytical model, which requires computer simulations. The current study is a continuation of that reported in [22]: (i) simulation algorithms are developed to produce three-dimensional microstructures as defined in the analytical model, and (ii) the effects of microstructure attributes, including composition, porosity, particle size (ratio), and particle morphology on TPB connectivity are studied.

2. Geometric simulations of three-dimensional porous composite electrode microstructures

2.1. Algorithm for simulations of microstructure with spherical powder particles (SPP)

Spatially isotropic uniform-random (IUR) three-dimensional (3D) microstructural volume segments are simulated. A composite electrode is simulated by placing electrode and electrolyte particles in a fixed cubic simulation box in an isotropic uniform-random way and the unoccupied space is porosity. IUR positioning means that the location of a particle is not affected by any other particle in the box, and that the no directionality exists other than the geometry of the simulation box itself. The number of electrolyte particles is specified by N^{EL} and electrode particles by N^{ED}. N^{EL} and N^{ED} are calculated so that desired composite cathode composition and porosity are achieved [22]:

$$\theta_P = \exp\left[-\left(N^{EL} V^{EL} + N^{ED} V^{ED} \right) \right] \quad (3)$$

$$\frac{\theta_{EL}}{\theta_{ED}} = \frac{N^{EL} V^{EL}}{N^{ED} V^{ED}} \quad (4)$$

where θ_P, θ_{EL} and θ_{ED} are the volume fractions of pores, electrolyte and electrode, respectively; V^{EL} and V^{ED} are the volumes of electrolyte and electrode particles, respectively.

In the special case when both electrode and electrolyte particles are spherical, the microstructure as described in [22] can be simulated by an efficient algorithm. In the analytical model, the particles are sequentially grown in small radial increments with growth rates proportional to their respective final sizes R^{EL} and R^{ED} in the microstructure till the final sizes are attained, respectively. The particles are allowed to freely grow on the canvas, allowing unlimited overlap, to simulate an "extended" microstructure. This process is conceptually similar to the evolution of an extended microstructure during a site saturated phase transformation where the particles of each constituent grow at a constant rate that is proportional to their final size [23,24]. During such microstructure evolution the ratio of the extended volume fractions of the electrolyte and cathode phase remains constant; let α be this ratio. Since the "extended" microstructure is physically untenable, it must be converted to "real" microstructure where the impingement among the particles in the extended microstructure is accounted for. It is possible to simulate the final microstructure by tracking each step of the incremental radial growth and converting the "extended" microstructure to "real" microstructure; it is, though, more efficient to directly simulate the final microstructure by finding out which how each phase occupy the space in the simulation box at the end of the process. Without loss of generality, let us assume $R^{EL} > R^{ED}$. A point P in the simulation box is labeled as the phase of the particle that *sweeps it first during the microstructure evolution*, or

$$L(P) = \arg\min_i \left(\frac{d^i(P)}{R^i} \right), \quad i \in \{EL, ED\}, \ d^i(P) \le R^i \quad (5)$$

[1] It is important to note that although not all active TPB is of equal catalytic activity in actual SOFC operation. A theoretic study [18] on the LSM–YSZ composite cathode has shown that a region close to the electrolyte contributes to the majority of the cathode current while the remaining cathode is less active, which is due to the limited ionic conductivity of porous YSZ. Therefore, this study focuses on the active TPB in an electrode of a limited and realistic thickness.

In Eq. (5), $L(P)$ is the label of P, with possible outcomes as EL, ED or porosity. $d^i(P)$ is the distance between the voxel P and its nearest neighboring particle of phase i, which can be EL or ED. R^i is the (final) radius of a particle of phase i. Eq. (5) yields the following rules for the conversion of extended microstructure to real microstructure.

1. If the point does not have any neighboring particle center up to distance R^{EL} ($R^{EL} > R^{ED}$), the voxel is labeled as porosity.
2. If there is no electrolyte particle center up to distance R^{ED} and there is at least one electrode particle center within distance R^{EL}, the voxel is labeled as EL.
3. If there is no electrode particle center up to distance R^{EL} and there is at least one electrolyte particle center within distance R^{ED}, the voxel is labeled as ED.
4. If the distances from the nearest neighboring EL and ED particle centers are both smaller than their corresponding radii, the point is assigned to the phase for which the ratio of its distance to the radius of the particle is smaller (according to Eq. (5)).

Fig. 2 shows a simulated composite electrode microstructure using spherical particles of same size for electrode and electrolyte phases.

2.2. Algorithm for simulations of microstructures with non-spherical convex powder particles (CPP)

While the SPP algorithm limits the particle morphology to sphere, slight modification will enable it to accommodate particles of any convex shape. First the particles are positioned IUR in the simulation box as in SPP; in addition, each particle is assigned three rotational degrees of freedom (DOF). The rotational DOF are assigned in two steps: (1) rotate the particle around its characteristics dimension axis by angle α; (2) rotate the characteristic dimension axis by spherical polar angle θ and ϕ with respect to external reference axes. Therefore, three angles (α, θ and ϕ) are needed to uniquely specify the orientation of a particle of an arbitratry convex shape. The rotational DOF must be randomly assigned so that the requirement of isotropy is[2] fulfilled in the simulated *global* microstructure. To achieve random rotation, an algorithm developed by Arvo [25] was used. Arvo's algorithm generates a rotational matrix $\mathbf{M}$ with three uniform-random inputs, so that $\mathbf{M}$ guarantees spatial orientation randomization. The geometry of a convex particle is specified by a set of column vectors designated by $\vec{\mathbf{R}}$ that gives the position vectors of the points on the surface of the particle. The rotated particle, designated by $\vec{\mathbf{R}}'$, is obtained by multiplying the column vector set $\vec{\mathbf{R}}$ by the matrix $\mathbf{M}$:

$$\vec{\mathbf{R}}' = \mathbf{M}\cdot\vec{\mathbf{R}} \tag{6}$$

The "real" microstructure having non-spherical convex particles can be recovered from the corresponding simulated extended microstructure using the steps similar to those used to simulate real microstructure with spherical particles. The phase assignment of a voxel P is therefore given as follows.

$$L(P) = \arg\min_i \left(\frac{d^i(P)}{R^i}\right), \quad i\in\{\mathrm{EL},\mathrm{ED}\}, \quad d^i(P) \le R^i \tag{7}$$

[2] The microstructure is required to be isotropic for Eq. (2) to be valid. This requirement is fulfilled in the simulations with spherical particles because spheres have inherent isotropy. Convex shapes particles, however, are not isotropic and therefore the microstructure isotropy must be introduced by orientation randomization.

R^i is the "radius" of the *rotated* particle of phase i (electrode or electrolyte) in the direction of the vector that starts at the center of the particle and ends at the voxel P (see Fig. 1). $d^i(P)$ is the distance vector between P and the nearest particle center of phase i. Eq. (7) assigns voxel P to the phase which has the smaller ratio of its distance to the voxel P and the directional radius R^i. Each voxel is assigned to EL, ED or porosity phases using the following rules.

1. If the voxel has no neighboring particle center to a distance of R^{EL} and R^{ED}, the voxel is labeled as porosity.
2. If there is no electrolyte particle center to a distance of R^{EL} and there is at least one electrode particle center within a distance of R^{ED}, the voxel is labeled as ED.
3. If there is no electrode particle center to a distance of R^{ED} and there is at least one electrolyte particle center within a distance of R^{EL}, the voxel is labeled as EL.
4. If the distances from the nearest neighboring electrode and electrolyte particle centers are both smaller than R^{EL} and R^{ED}, respectively, the voxel is labeled according to Eq. (7).

Figs. 3 and 4 are simulated composite electrode microstructures using needle-shaped and plate-like particles, respectively.

2.3. Quantitative analysis of TPB connectivity

In a 3D microstructure, a TPB is a lineal microstructure feature connected to the three phases, gas porosity, electrolyte phase, and electrode phase. Therefore, TPBs can be identified in the simulated microstructure by inspecting the surroundings of each point (pixel) in the simulation box.

A *topologically connected* TPB segment is the TPB segment that forms a connected path between the top (say current collector/porosity) and the bottom (say electrolyte) of the SOFC. Such topologically connected TPB segments can be identified by using connected component labeling algorithm of digital image processing [26]. For this purpose, a layer of current collector/gas pore is attached to one side of the cathode and a layer of electrolyte is

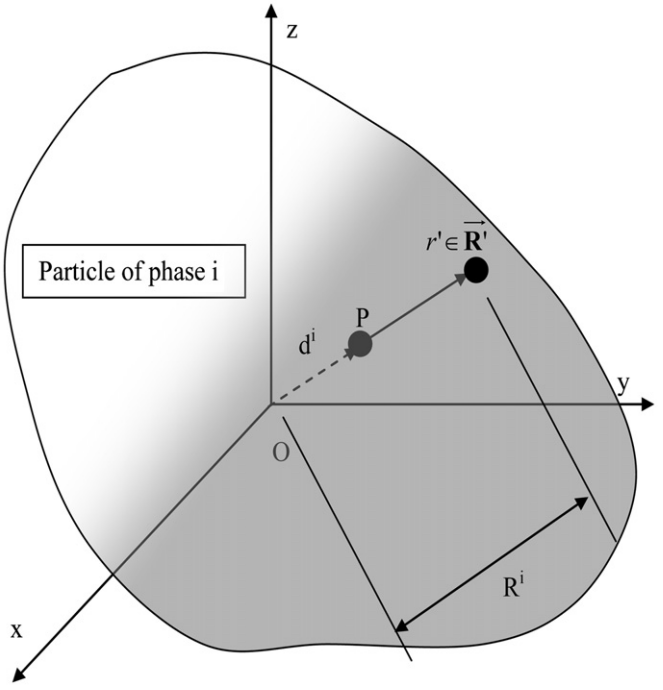

Fig. 1. Depiction of the geometric relationship in Eq. (7)

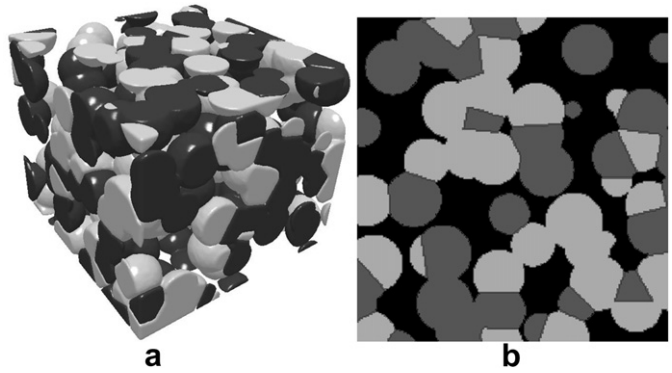

Fig. 2. A segment of a simulation microstructure of a composite electrode with 40% porosity, electrolyte and electrode phases of each volume fraction and particle size. (a) The surface rendered 3D microstructure; (b) a cross-section of (a).

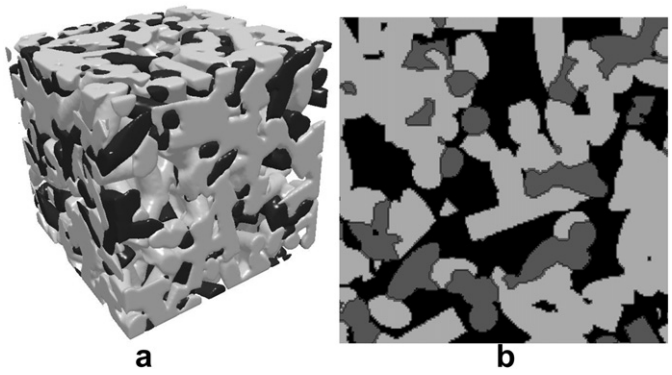

Fig. 3. A segment of a simulation microstructure of a composite electrode with 27% porosity, 51% electrode phase (white) and 22% electrolyte phase (gray), both comprises needle-shaped particles ($L/R = 9$) of equal size. (a) The surface rendered 3D microstructure; (b) a cross-section in (a).

attached to the opposite side (see Fig. 5). Using the connected component labeling technique, a point in the electrode phase or the gas pore is defined as "connected" if it has a conducting path to the current collector side.[3] Likewise, a point in the electrolyte phase is considered "connected" if it has a conducting path to the electrolyte side. A TPB site is only regarded as topologically connected if the three phases that forms it are all labeled "connected".[3] The fraction of connected TPB is then calculated by dividing the connected TPB by the total length of TPB. A C++ code was developed to measure the total and connected length of TPB [27]. It should be noted that the length of TPB, total or connected, is measured using the stereological principle that the length of a linear feature per unit volume is equal to twice the number of intercepts of the feature with sectioning planes per unit area:

$$L_{\mathrm{TPB}} = L_{\mathrm{V}} = 2\frac{\langle N_{\mathrm{TPB}}\rangle}{A} \tag{8}$$

where N_{TPB} is the number of pixels identified as TPB on each layer of pixels (with area A) in the simulation box. For total length of TPB, all TPB pixels are counted towards N_{TPB}; for connected length of TPB, only those neighboring connected gas pore, electrolyte, and electrode phases are connected towards N_{TPB}.

[3] In a planar cathode configuration, the cathodic current collector is on the same side of the cathode as the supply of air or oxygen. Such geometry also applies to the planar anode.

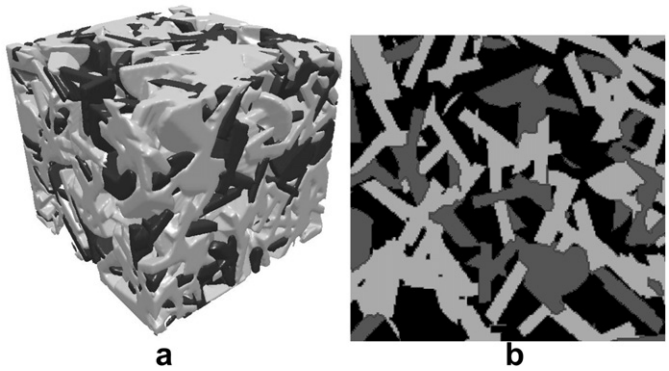

Fig. 4. A segment of a simulation microstructure of a composite electrode with 27% porosity, 51% electrode phase (white) and 22% electrolyte phase (gray), both comprises needle-shaped particles ($L/R = 1/3$) of equal size. (a) The surface rendered 3D microstructure; (b) a cross-section in (a).

To understand the effects volume fractions of the constituent phases, sizes, and particle morphologies on the connectivity of the TPBs, a large number of simulated microstructures were generated and analyzed by the aforementioned procedure.

3. Results and discussion

3.1. Validation of microstructure simulations

Since SPP and CPP are designed to generate three-dimensional implementations of the analytical microstructure model, the simulations that they produce must matches quantitatively with the analytical calculations of the model. In Fig. 6 it is shown that the total length of TPB calculated by Eq. (2) matches wells with that stereologically measured from the SPP simulations. It should be noted that each point in Fig. 6 represents the average of eight instances of simulation. The simulations in Fig. 6 have varying process parameters with porosity of 5–30%, composition of 30–70% electrolyte phase and particle size ratio (PSR) of 1:1 to 5:1. Fig. 7 shows SPP having particle morphologies ranging from needles to plates also matches well with model calculation, with marginal errors attributed to pixilation. The verified simulations allow parametric studies of TPB topological connectivity.

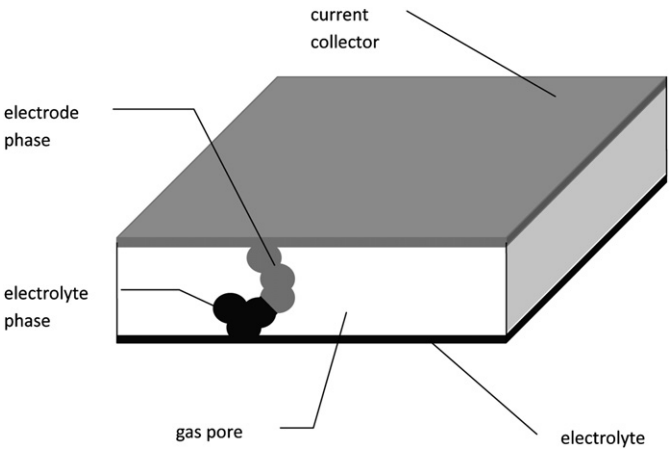

Fig. 5. Configuration of the simulated planar composite cathode. The electrode phase in the composite and the gas pore are defined "connected" if they have at least one path to the current collector. The electrolyte phase in the composite is defined "connected" if it has at least one path to the electrolyte.

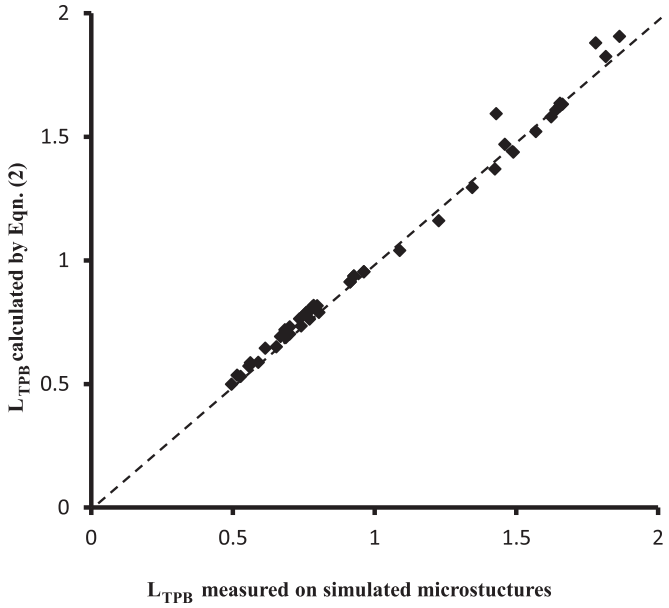

Fig. 6. L_{TPB} measured in the SPP simulation (x axis) and calculated by Eq. (2) (y axis). The dashed line is $y = x$.

3.2. Effects of composition

Microstructure with varying compositions have been simulated and quantified. For each composition, eight instances were generated to provide sufficient sampling. In this parametric study the particle sizes of electrode and electrolyte phases are identical and the particles are spherical. The size of the simulated microstructure is equal to 18 times the particle radius.

The effects of volume fractions of electrolyte and electrode phases are determined by studying how the percentage of connected TPB varies with composition when porosity, particle size and morphology remain unchanged. Fig. 8 is a plot of the percentage of connected TPB in simulations with the porosity level of 27%. Obviously the highest TPB connectivity is achieved with

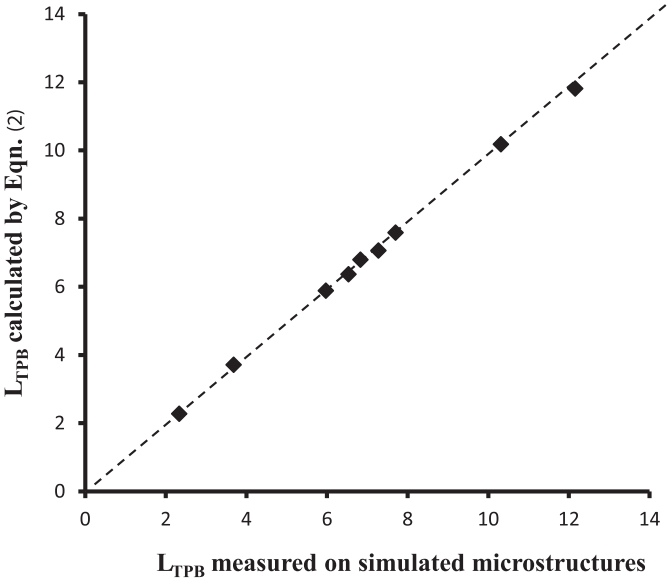

Fig. 7. L_{TPB} measured in the CPP simulations (x axis) with cylindrical particles and calculated by Eq. (2) (y axis). The dashed line is $y = x$.

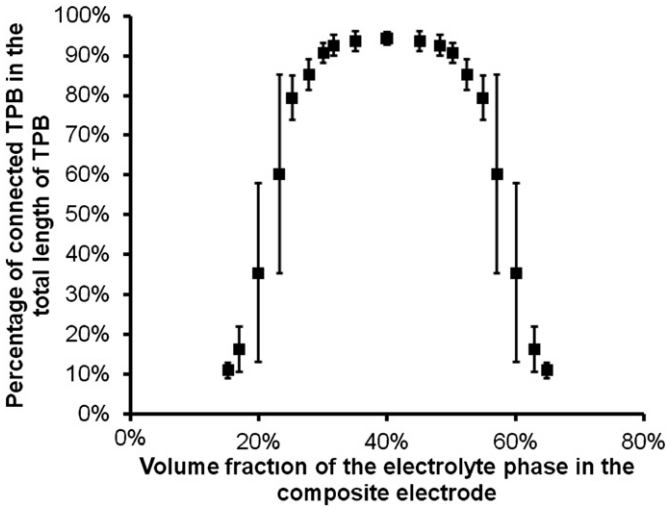

Fig. 8. The variation of connected TPB with volume fraction of the electrolyte phase when the porosity volume fraction is 27%.

equal volume fractions (36.5%) of the solid constituents. Since the porosity volume fraction is constant, the variation of the connected TPB is attributed to the change of volume fractions of the electrode or electrolyte phases. When the volume fraction of electrolyte phase is below 36.5%, the connected TPB increases with increasing volume fraction of the electrolyte phase, which is due to the percolation of the electrolyte phase. Beyond the volume fraction of 36.5%, the connectivity of TPB decreases symmetrically due to the loss of percolation of the electrode phase. The connectivity of TPB increases rapidly when the volume fraction increases above 17%, where the electrolyte phase begins to percolate. The rapid increase of connectivity of TPB is accompanied by large standard errors due to the instability of connectivity of TPB to local microstructure. After the volume fraction increases to 30%, the connectivity of TPB saturates. The percolation threshold of the electrolyte phase is therefore between 20% and 30%, when the porosity volume fraction is 27%.

Simulations with other porosity volume fractions are performed. It is shown in Fig. 9 that when the porosity volume fraction is reduced from 27% to 20%, the percolation thresholds decrease from 30% to 23% for either electrode or electrolyte phase.

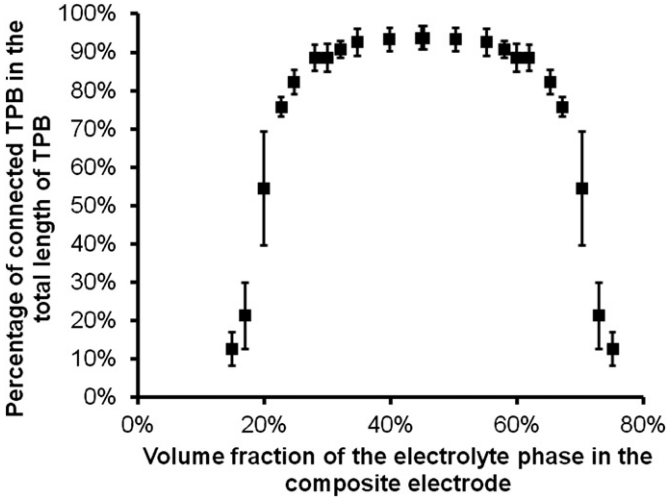

Fig. 9. The variation of connected TPB with volume fraction of the electrolyte phase when the porosity volume fraction is 20%.

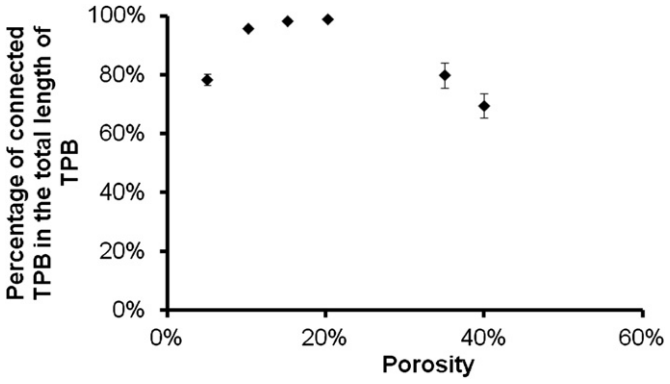

Fig. 10. The variation of TPB connectivity with porosity volume fractions when the volume fractions of electrolyte phase and electrode phase are equal.

3.3. The effect of porosity

The effect of the volume fraction of porosity is assessed by varying porosity while keeping equal volume fractions of solid constituents. Fig. 10 is a plot of the percentage of connected TPB in simulations with equal volume fractions of solid constituents. The most notable feature of Fig. 10 is that the lack of symmetry around any porosity volume fractions as in Figs. 8 and 9, which indicates that the percolation behavior of porosity is different from that of the electrolyte or electrode phase. In addition, Fig. 10 shows that the percolation threshold of porosity is 5–10%, which is significantly lower than that of the solid constituents (22–32%). Indeed, the lower percolation threshold reflects the topological characteristics of a Boolean microstructure model [28]. In the Boolean model the phase that is added into the canvas usually has a percolation threshold about 20–30%. However, the unfilled space has a typical percolation threshold of about 6% [28]. The physical implication is that 5–10% porosity suffice to form an interconnected network of pore channel. Nonetheless, a higher porosity might be more favorable so that mass transfer is not impeded by the pore channel conductivity. Furthermore, Gokhale and Zhang's model suggests that 13.5% porosity yields the higher length of TPB, which might be a reasonable reference for the selection of process parameters.

Fig. 10 also reveals the effects of higher porosity. As the porosity increases beyond 35%, the connected TPB decreases steadily because the remaining volume fractions of electrode or electrolyte phases become insufficient to percolate. Furthermore, the percolation threshold itself is increased as the porosity volume fraction increases, as was discussed previously.

3.4. Combined effects of porosity and composition

The study on composition has led us to the conclusion that at a certain porosity volume fraction, the maximum TPB connectivity is achieved when the volume fractions of constituents are equal. It is also found that increasing porosity makes TPB less connected. To clarify the role of porosity, another set of simulations are generated and quantified. It is found that that the percolation threshold of porosity is about 5–10% and increasing porosity reduces TPB connectivity by compromising the connectivity of constituents.

These parametric studies suggest a strong correlation between porosity and composition. A ternary contour plot is used to present all simulation results. The coordinate of a point in the ternary plot (Fig. 11) gives the volume fractions of electrolyte phase, electrode phase and porosity. The contour line marks levels of TPB connectivity in terms of percentage. The ternary plot can serve as guidelines for the selection of composition and porosity for composite cathodes/anodes.

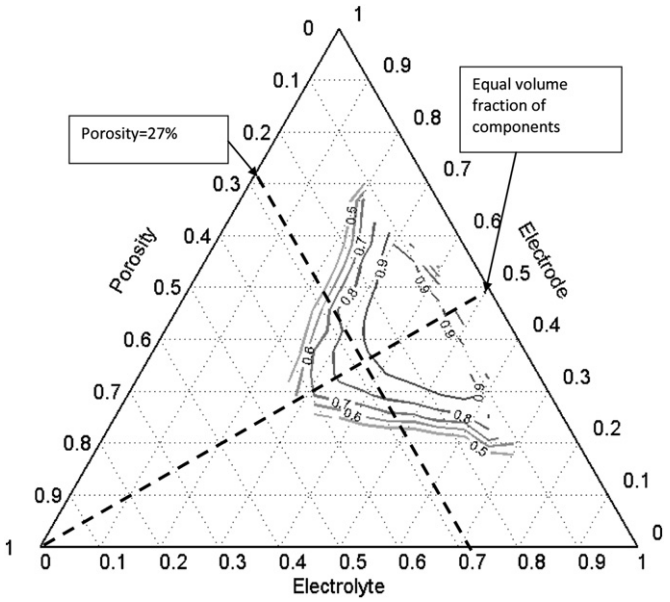

Fig. 11. Ternary contour plot of the fraction of the length of connected TPB in the length of total TPB. Spherical particles of the two components have the same radius. The thickness of the electrodes is 18 times the particle radius.

3.5. Particle size effect

The effects of particle sizes on topological connectivity may be deconvoluted into the effects of two parameters: particle size ratio (PSR) and relative electrode thickness with respect to particle sizes. The two parameters are studied with different sets of simulations. The effects of PSR are studied with simulations of 5 different particles size ratios and the results are plotted in Fig. 12. The effects of thickness are quantified by varying the thickness of the simulated electrode.

It is revealed in Fig. 12 that PSR does not affect the topological connectivity in any significant manner. There is no obvious trend in the percentage of connected TPB with increasing or decreasing PSR. Since the simulations cover a wide of particle size ratios that are of

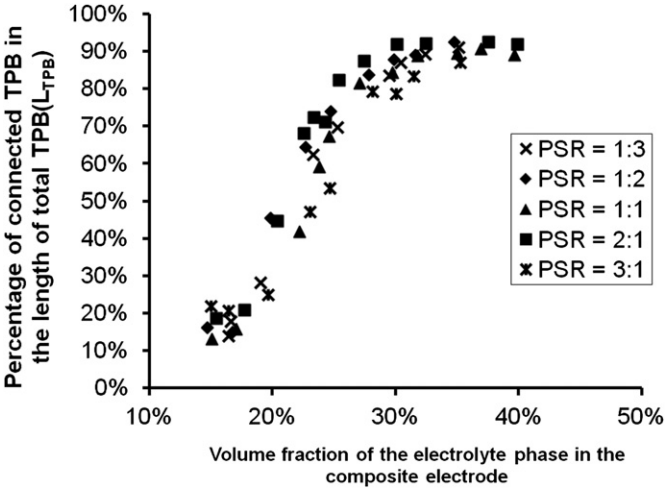

Fig. 12. Dependence of the connectivity of TPB on particle size ratios.

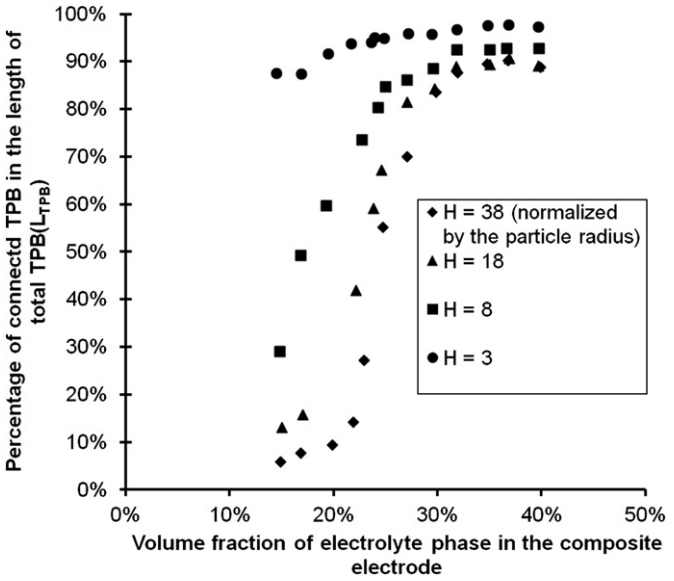

Fig.13. The variation of percentage of active TPB with volume fraction of electrolyte phase in simulated electrodes of different normalized thicknesses.

practical importance (1:5 to 5:1), it is reasonable to suggest that PSR is not a potent factor for the connectivity of TPB.

The thickness of an electrode, on the other hand, has a pronounced effect of the topological connectivity of TPB. Fig. 13 shows that the percentage of connected TPB increases with decreasing thickness. When the thickness is about 1.5 particle diameter, a high percentage (>80%) of TPB is connected regardless of the composition. The connectivity of TPB generally decreases with increasing thickness until a certain thickness is reached (~20 particle diameter), above which the connectivity characteristics approximate that of an electrode of infinite thickness.

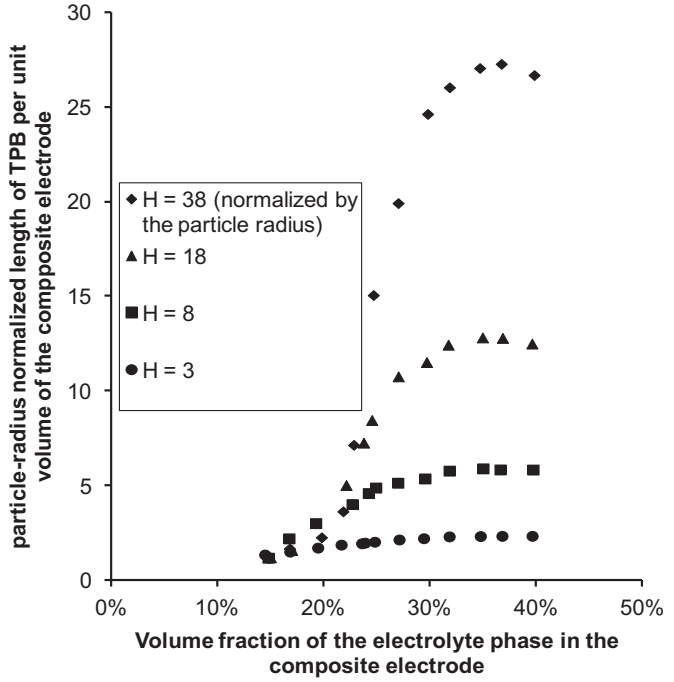

Fig. 14. Length of connected TPB per unit area of the composite electrode for different thicknesses.

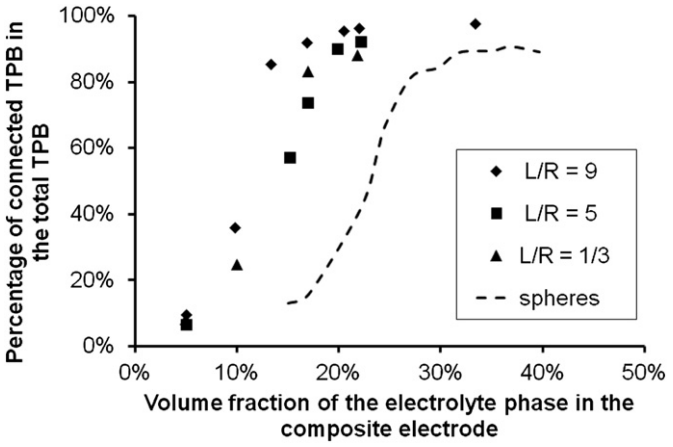

Fig. 15. The percentage of connected TPB in the composite electrode with cylindrical particles of different height–radius ratios (L/R), with 27% porosity. Dashed line is the percolation of TPB in microstructure composed of spherical particles with the same porosity.

Even though reducing the thickness of a composite electrode will increase the connectivity of TPB, it is important to note that the total length of TPB decreases proportionally with thickness. The reduction in total length of TPB due to thickness reduction cancels the increases in connectivity of TPB for most compositions, as shown in Fig. 14. Reduction in thickness only increases the length of connected TPB when the composition of either component is close to or below the percolation threshold.

3.6. *Effects of particle morphologies*

The morphology of particles not only affects the total length of TPB, as predicted in [22], but also has substantial effects on the connectivity of TPB. To study the effect of particle morphologies, three series of simulations were performed using cylindrical particles of different height-radius ratios (height/radius = 9, 5 and 1/3), representing needle-shaped (whisker) and plate-shaped (flake) particles, respectively. The percentage of connected TPB is plotted against the volume fraction of the connectivity-limiting component (e.g. electrode phase) (Fig. 15). In the plot all three simulations achieve over 80% connected TPB when the volume fraction is above 20%, which makes the percolation threshold volume fraction 10–20%. Recall in the previous study the percolation thresholds of electrolyte or electrode phases were determined to be 20–30%. We can therefore conclude that non-spherical convex-shaped particle morphology will reduce the corresponding percolation threshold and increase topological connectivity TPB. This also implies that the previous discussions on the fractions of connected TPB give the *lower bound* of the actual connectivity, since the spherical particle morphology leads to the lowest TPB connectivity.

4. Conclusion

The topologically activity of the TPB in the stochastic geometry based model developed for the SOFC composite cathodes has been quantified by connected component labeling analysis and stereological measurements on microstructure simulations. Several parameters have been studied for their effects on the activity on the TPB and following conclusions are drawn from the studies.

1. The gas pores are topologically connected as long as the porosity of the cathode is above 10%.

2. The connectivity threshold for a constituent (electrolyte or electrode phase) is about 25%. More than 87% of the TPB becomes active if both constituents have volume fraction above 30%.
3. The activity of TPB decreases with the particle size of a constituent when the volume fraction of the constituent is below the connectivity threshold. The connectivity threshold does not exhibit significant dependence on particle size. These conclusions are valid for a moderate range of PSR (PSR < 5).
4. Reducing the thickness of a composite cathode will improve the topological activity of the TPB especially when either of the constituent has a volume fraction below the connectivity threshold. However, when the total active TPB length/active TPB length per unit area is concerned, a thicker cathode is more favorable when volume fractions of both constituents are above 25%.
5. Using non-equiaxed particles increases connectivity and reduces the percolation threshold to 10–20%. Lowest connectivity corresponds to spherical particles, therefore all connectivity analyses based on spherical particles gives the lower bound of TPB connectivity.
6. The prediction of Eq. (2) as proposed in the previous contribution is valid for the topologically active TPB length if the volume fractions of both constituents are above 30% and the porosity is above 10%.

Acknowledgement

This research was supported through a grant from the U.S. National Science Foundation (NSF grant DMR-0813630) for which Dr. B. MacDonald and Dr. A. J. Ardell are the Program Managers. The financial support is gratefully acknowledged. The views and conclusions contained herein are those of the authors and should not be interpreted as necessarily representing the official policies or endorsements, either expressed or implied, of the funding agency or the US government.

References

[1] R.M. Ormerod, Chemical Society Reviews 32 (2003) 17–28.
[2] B.C.H. Steele, A. Heinzel, Nature 414 (2001) 345–352.
[3] V. Brichzin, J. Fleig, H.U. Habermeier, G. Cristiani, J. Maier, Solid State Ionics 152, 153 (2002) 499–507.
[4] T. Horita, K. Yamaji, N. Sakai, H. Yokokawa, T. Kawada, T. Kato, Solid State Ionics 127 (2000) 55–65.
[5] M.J. Jorgensen, S. Primdahl, C. Bagger, M. Mogensen, Solid State Ionics 139 (2001) 1–11.
[6] W.G. Wang, Y.L. Liu, R. Barfod, S.B. Schougaard, P. Gordes, S. Ramousse, P.V. Hendriksen, M. Mogensen, Electrochemical and Solid State Letters 8 (2005) A619–A621.
[7] V. Dusastre, J.A. Kilner, Solid State Ionics 126 (1999) 163–174.
[8] M.J. Jorgensen, M. Mogensen, Journal of the Electrochemical Society 148 (2001) A433–A442.
[9] M. Juhl, S. Primdahl, C. Manon, M. Mogensen, Journal of Power Sources 61 (1996) 173–181.
[10] E.P. Murray, S.A. Barnett, Solid State Ionics 143 (2001) 265–273.
[11] S. Sunde, Journal of the Electrochemical Society 143 (1996) 1930–1939.
[12] S. Sunde, Journal of Electroceramics 5 (2000) 153–182.
[13] L.C.R. Schneider, C.L. Martin, Y. Bultel, D. Bouvard, E. Siebert, Electrochimica Acta 52 (2006) 314–324.
[14] X.J. Chen, S.H. Chan, K.A. Khor, Electrochimica Acta 49 (2004) 1851–1861.
[15] A. Abbaspour, K. Nandakumar, J.L. Luo, K.T. Chuang, Journal of Power Sources 161 (2006) 965–970.
[16] Y. Ji, K. Yuan, J.N. Chung, Journal of Power Sources 165 (2007) 774–785.
[17] C. Metcalfe, O. Kesler, T. Rivard, F. Gitzhofer, N. Abatzoglou, Journal of the Electrochemical Society, 157 B1326–B1335.
[18] S. Sunde, Journal of the Electrochemical Society 143 (1996) 1123–1132.
[19] A. Ali, X. Wen, K. Nandakumar, J. Luo, K.T. Chuang, Journal of Power Sources 185 (2008) 961–966.
[20] B. Kenney, M. Valdmanis, C. Baker, J.G. Pharoah, K. Karan, Journal of Power Sources 189 (2009) 1051–1059.
[21] S.P. Jiang, Journal of Power Sources 124 (2003) 390–402.
[22] A.M. Gokhale, S. Zhang, M. Liu, Journal of Power Sources 194 (2009) 303–312.
[23] M. Avrami, Journal of Chemical Physics 7 (1939) 1103–1112.
[24] M. Avrami, Journal of Chemical Physics 9 (1941) 177–184.
[25] J. Arvo, in: D. Kirk (Ed.), Graphics Gems III, Academic Press, New York, 1992, pp. 117–120.
[26] E. Tola (2006) Available from: http://cvlab.epfl.ch/~tola/index.html (accessed 4/23/2009).
[27] S. Zhang, Ph.D. dissertation, School of Materials Science and Engineering, Georgia Institute of Technology, Atlanta, GA (2010).
[28] C.D. Lorenz, R.M. Ziff, The Journal of Chemical Physics 114 (2001) 3659–3661.